DETERMINATION OF THE SOOTBLOWER ACTIVATION MOMENT FOR BIOMASS CO-FIRING IN A PULVERIZED COAL FURNACE

by

Nenad Dj. CRNOMARKOVIĆ[a*], Srdjan V. BELOŠEVIĆ[a], Stevan Dj. NEMODA[a], Ivan D. TOMANOVIĆ[a], Aleksandar R. MILIĆEVIĆ[a], Andrijana D. STOJANOVIĆ[a], and Goran M. STUPAR[b]

[a] Department of Thermal Engineering and Energy, Vinča Institute of Nuclear Sciences,
National Institute of the Republic of Serbia, University of Belgrade, Belgrade, Serbia
[b] Faculty of Mechanical Engineering, University of Belgrade, Belgrade, Serbia

The pulverized coal-fired furnaces are expected to use co-firing with biomass for environmental reasons. Although the non-uniform ash deposits are formed on the furnace walls, the uniform deposits could be used for the analysis of the furnace operation. The objective of this investigation was determination of the uniform deposit thickness, used as a criterion for prediction of the sootblower activation moment in coal-biomass co-firing. The investigation comprised numerical simulations for uniform and non-uniform deposits to find the relative differences for the selected variables that were important for the sootblower activation: the mean wall fluxes and flame temperatures. The local thicknesses of the non-uniform deposits were determined by the gamma distribution for several mean and standard deviation values using the inversion method. The thicknesses of the uniform deposits were considered among the measures of central tendency: mode, mean, and median, of the non-uniform deposits. The mean was expected to provide the smallest relative differences, while the mode was excluded from further consideration after analysis of its values. The median was found to be better choice than the mean, as it provided smaller relative differences of the selected variables for the thick deposits, which were important for the sootblower activation. The method based on comparison of the uniform deposits for coal firing and those for the co-firing with biomass was proposed for the prediction of the sootblower activation moment. The method can be used for the selection of the operational regimes for coal-biomass co-firing.

Key words: *numerical investigation, furnace, ash deposit, mean, median, mode, standard deviation*

Introduction

Nowadays, the pulverized coal boilers are expected to use co-firing with biomass for energy production. Biomass is used as a secondary fuel and replaces up to 20% of coal (thermal input). Co-firing reduces emission of the carbon-dioxide, as well as nitrogen and sulfur oxides [1-3]. The main problem in the use of biomass is its alkali content in ash, such as potassium and sodium, whose compounds (oxides, hydroxides, chlorides and sulfates) and some eutectic mixtures melt at low temperatures [4, 5] and are easily deposited on the furnace walls. Wheat straw,

---

used as an example of the agricultural biomass, contains more potassium than oak wood, used here as an example of the forest biomass. Potassium in the agricultural biomass is present from fertilizers [5]. Alkali oxides act as a bonding agent for deposited ash particles, in two ways: by condensing on the surfaces of the particles and heating surfaces, and by making the eutectic mixtures of low melting temperature, which increase the deposit sintering. Generally, ash fusibility temperatures are the lowest for the agricultural biomass. Some of the basic properties of the selected coal and biomasses are given in tab. 1.

Table 1. Basic properties of the Kolubara lignite and selected biomasses [5-7]

Property	Lignite Kolubara	Wheat straw	Oak wood
Ash [db, wt.%]	28.66	12.8	0.50
LHV [db, MJkg^{-1}]	17.455	16.55	–
Ash composition			
SiO_2 [%]	52.17	50.35	48.95
Al_2O_3 [%]	22.31	1.54	9.49
TiO_2 [%]	0.73	0.09	0.10
Fe_2O_3 [%]	6.35	0.88	8.49
MgO [%]	2.76	2.74	1.1
CaO [%]	8.35	8.21	17.48
Na_2O [%]	0.49	3.52	0.50
K_2O [%]	1	24.89	9.49
P_2O_5 [%]	0.12	3.54	1.8
SO_3 [%]	5.69	4.24	2.6
Ash temperatures			
Shrinkage starting [K]	–	1153	1399
Deformation [K]	1460	1193	–
Hemisphere [K]	1609	1373	1487
Fluid [K]	1630	1433	1494
Slagging index			
Base-acid ratio [–]	0.25	0.77	0.63
Silica ratio [%]	74.9	80.97	64.39
Silica-alumina ratio [–]	2.34	32.69	5.16
Iron-dolomite ratio [–]	0.57	0.08	0.46
Iron-calcium ratio [–]	0.76	0.11	0.49
Dolomite percentage [%]	58.63	27.21	50.13

The ash deposits on the furnace walls affect not only heat transfer in the furnace but also in the whole boiler [8]. Ash deposition reduces the heat transfer ability of the furnace and reduces the radiative heat exchange between the flame and walls and increase the flame temperatures. An increase in the flame temperature above certain limits causes fouling of the superheaters located near the furnace exit. An increase in the gaseous combustion products temperature in the convective duct increases the steam temperature, which makes it more difficult to control. The increase of the boiler exhaust gases temperature decreases the boiler efficiency. Plaza *et al*. [9] showed that the co-firing coal with sewage sludge with a thermal share of 20%

increased the boiler exit gas temperature by 50 K and reduced the efficiency of the boiler by 4%. Finally, the increase in flame temperature increases the NO emission, through the formation of thermal NO, whose formation is important at temperatures above 1650 K [10]. Much more important source of the NO is oxidation of the nitrogen fuel, but this mainly depends on combustion stoichiometry.

Propensity of pulverized coal ashes to form deposits on the furnace walls (*i.e.* slagging) can be estimated from various indexes based on ash composition or ash fusibility temperatures. Some of these indexes for the selected coal and biomasses are presented in tab. 1. The indexes based on the ash composition estimate the ash fusibility temperatures of ash viscosity: the lower fusibility temperature or viscosity, the higher propensity to form deposits. The use of the indexes for the biomass fuel is questionable because of the differences in inorganic constituents. Inorganic constituents in coal are mainly in the form of the minerals, while in biomass they are organically bound elements or in the free ionic form [11]. Similarly, the indexes based on ash composition does not include the form of alkalies in fuel: active and inactive alkalies [12]. Active alkalies are organically bound alkalies and simple salts, which vaporize during combustion and condense on the heating surfaces. Inactive alkalies are constituents of clays and shale minerals and do not influence the process of deposit formation. Alkalies in biomass ashes are mainly in the active form. For the coal-biomass blends, the modified slagging index developed by Degereji *et al.* [13] or SI index developed by Kupka *et al.* [14] can be used. The investigation conducted by Degereji *et al.* [13] showed that the propensity of coal-biomass blends to make deposits on the heating surfaces is not necessarily bigger than for the case of coal firing. That was also experienced by the field measurements [15].

The investigation of the deposition rate corresponding to the slagging conditions for coal and coal biomass blends was performed by Kupka *et al.* [14]. The biomass share was not bigger than 20% (heat input) and biomasses included sewage sludge, saw dust, and refuse derive fuel. Deposition rates for coal-sewage sludge and coal-refuse derive fuel co-firing were bigger than for coal firing, whereas those for the coal-saw dust co-firing were smaller than for coal firing. The deposition rates were measured for two gas temperatures: 1573 and 1473 K. At 1473 K, the deposition rates were almost always the half of those for 1573 K.

The ash deposits are removed from the furnace walls by the sootblowers, such as the short retractable sootblower and waterlance, which uses compressed air, steam (saturated or superheated), and boiler water as the blowing medium. The impact of the ash deposits on the furnace operation and the moment for the activation of the sootblowers can be predicted by the numerical simulations [16, 17], in which the local deposit thicknesses are determined. The thickness of the non-uniform deposit (ND) is determined in time and the sootblowers should be activated when a certain criterion is reached, such as the value of the heat exchanged between the flame and furnace walls or temperature level at the furnace exit. The impact of the ash deposits on the furnace operation can also be found by the uniform deposits (UD) [18, 19]. In that case, the criterion for the sootblower activation could be the UD thickness.

Objective of this investigation is determination of the UD thickness, as a criterion for prediction of the sootblower activation moment for coal-biomass co-firing. Numerical simulations of a utility boiler furnace for both types of deposits are conducted and the relative differences (RD) of the selected variables are found, important for determination of the sootblower activation moment. The UD thickness is determined as the corresponding thickness of the ND, which provides the smallest difference of the selected variables. The local ND thicknesses are formed by means of the gamma distribution, used as an example of asymmetric distribution that gives different values of the measures of central tendency, for several mean and standard deviation val-

ues. The thicknesses of the UD are selected among the measures of central tendency of the ND: mode, mean, or median. The expected result of the investigation is formulation of the method for determination of the sootblower activation moment in the furnace for coal-biomass co-firing.

For this investigation, the furnace of a 210 MWe monobloc thermal unit was selected. The furnace is tangentially fired by Kolubara lignite and equipped with six jet burners (four tiers each), five of which are in operation. The prismatic shape is 40 m high, 15.5 m wide, and 13.5 m deep. Details of the furnace geometry, flow rates of the air and coal, as well as coal properties, were given in [20]. The mathematical model of the flow and thermal processes inside the furnace, the results, and the conclusions of this research are described below.

The mathematical model of the furnace processes

The mathematical model of the processes inside the furnace described a two-phase, turbulent reacting flow with radiative heat exchange. The gas phase was described by the time-averaged differential equations of the conservation of the momentum, enthalpy, species concentrations, turbulent kinetic energy, and dissipation rate of turbulent kinetic energy, in the Eulerian reference frame. The general form of the gas-phase equation:

$$\text{div}\left(\rho \vec{\mathbf{U}} \Phi\right) = \text{div}\left(\Gamma_\Phi \text{grad}\,\Phi\right) + S_\Phi + S_{\Phi,p} \tag{1}$$

where ρ [kgm^{-3}] is the gas-phase density, $\vec{\mathbf{U}}$ [ms^{-1}] – the gas-phase velocity, Φ – the general variable of the gas phase, Γ_Φ [kgm^{-1}s^{-1}] – the transport coefficient for Φ, S_Φ – the source term for Φ, and $S_{\Phi,p}$ – the source term for Φ due to the presence of particles. The set of equations was closed by a *k-ε* turbulence model. The pressure field was solved by the SIMPLE algorithm. The equations of the mathematical model were solved for the thermal equilibrium between gas and dispersed phases [21].

The dispersed phase was described by the differential equations of the motion and change of mass and energy in the Lagrangian reference frame. Motion of the particles was tracked along trajectories with a constant flow of particles. Connection between the gas and dispersed phases was achieved by the PSI CELL concept, by which the presence of particles was taken into account as additional source terms in the gas-phase equations. The particle velocity vector was a sum of the convective and diffusion components. Heterogeneous reactions of coal combustion were modeled in the kinetic-diffusion regime [22].

Radiative heat exchange was solved using the zonal model of radiative heat transfer [23]. The wall flux of the surface zone s_i was determined:

$$q_{\text{w},i} = \frac{\displaystyle\sum_{m=1}^{M} G_i S_i \sigma_{\text{SB}} T_{\text{f},m}^4 + \sum_{n=1}^{N} S_n S_i \sigma_{\text{SB}} T_{\text{w},n}^4 - \epsilon_{\text{w},i}\sigma_{\text{SB}} T_{\text{w},i}^4}{A_i} = \frac{Q_i}{A_i} \tag{2}$$

where $G_m S_i$ [m^2] is the volume-surface total exchange area, $S_n S_i$ [m^2] – the surface-surface total exchange area, M – the total number of the volume zones, N – the total number of the surface zones, σ_{SB} [WK^{-4} m^{-2}] – the Stefan-Boltzmann constant, ϵ_{w} [–] – the wall emissivity, T_{f} [K] – the flame temperature, T_{w} [K] – the wall temperature, A [m^2] – the surface area, and Q [W] – the heat transfer rate. The mean wall flux was obtained by $\overline{q}_{\text{w}} = Q_{\text{tot}}/A_{\text{fw}}$ where Q_{tot} [W] – the total radiative heat exchange in the furnace, obtained by the summation of all heat transfer rates for the surface zones as the solid walls, $Q_{\text{tot}} = \sum Q_i$, and A_{fw} [m^2] is the total surface area of the furnace walls.

The furnace waterwall was a series composite wall, composed of a 4 mm thick metal wall and the deposit layer. One boundary surface of the furnace wall (boundary surface of

the metal wall) was exposed to the water-steam mixture, whereas the other boundary surface (boundary surface of the deposit layer) was exposed to the flame. The temperature of the wall boundary surface exposed to the flame was the wall temperature, T_w, in the mathematical model.

The temperature of the water-steam mixture was determined for the boiling water according to its pressure, $T_b = 615$ K. The wall temperature was determined using the 1-D steady-state heat conduction equation:

$$T_w = T_b + q_{w,i}\left(\frac{1}{h} + \frac{l_m}{K_m} + \frac{l_d}{K_d}\right) \tag{3}$$

where h [Wm^{-2}K^{-1}] is the convection heat transfer coefficient, K_m [Wm^{-1}K^{-1}] – the thermal conductivity of the metal wall, K_d [Wm^{-1}K^{-1}] – the thermal conductivity of the deposit, l_m [mm] – the thickness of the metal wall, and l_d [mm] – the thickness of the deposit. The dependences of K_d and ϵ_w on temperature were adopted from [24]. For determination of K_d, the ash sample was ground to the pulverized size and put in the crucible in the form of layer. The layer of the ash was heated from one side, and the effective thermal conductivity of the ash deposit was determined from the measurements of the heat fluxes and temperatures.

The zonal model of thermal radiation was applied through the continual corrections of the total exchange areas (CCTEA) method [25]. The total surface areas were determined for the initial value of the surface emissivity and changed according to the wall temperature. The method is based on the correction of the total exchange areas, in accordance with the values of the surface zone emissivity and summation principle. Thermophysical properties were determined from the equation of state, tabulated values, and empirical relations. Discretization and linearization of the gas-phase equations were achieved by a method of control volumes and hybrid differencing scheme. Stability of the iterative procedure was provided by the under-relaxation method.

The probability density function of the gamma distribution was given [26]:

$$f(l_d) = l_d^{\alpha-1}\frac{\exp\left(-\dfrac{l_d}{\beta}\right)}{\beta^\alpha\Gamma(\alpha)} \tag{4}$$

where α [–] and β [mm] are the distribution coefficients and $\Gamma()$ – the gamma function. The distribution coefficients were determined from the parameters $\beta = \sigma^2/\mu$ and $\alpha = \mu/\beta$ [26], where μ [mm] is the mean and σ [mm] – the standard deviation. The local deposit thickness l_d was determined by the inversion method [27]. First, the number of cumulative distribution function $F(l_d)$ values was found using Keisan online calculator [28] for every pair of the distribution parameters, and the local deposit thicknesses were determined from the condition $F(l_d) = \zeta$, where ζ [–] is the uniformly distributed random number determined by the congruential generator [29]. For one particular μ value, σ values were selected from the condition $\sigma < \mu$. For $\mu = 1$ mm, the maximal σ value was such that it did not require the adjustment of the computer code. The selected standard deviations were in the interval from 0.05-0.5 mm. The median values were determined from the condition:

$$\int_0^{\tilde{\mu}} f(l_d)\mathrm{d}l_d = 0.5$$

and given in tab. 2, which showed that the median decreased with an increase in the standard deviation. The median values were smaller than the corresponding mean values.

Table 2. The median values $\tilde{\mu}$ [mm]

μ [mm]	σ [mm]					
	0.05	0.1	0.2	0.3	0.4	0.5
0.25	0.247	0.237	0.199			
0.35	0.348	0.34	0.313	0.269		
0.5	0.498	0.493	0.474	0.441	0.398	
1	0.999	0.997	0.987	0.97	0.939	0.918

The mode values were determined from the condition $\mathrm{d}f/\mathrm{d}l_d = 0$, which results in $\hat{\mu} = \beta(\alpha - 1)$, and were given in tab. 3. The mode was smaller than the corresponding median, and the difference increased with the increase in the standard deviation. If $\mu = \sigma$, then $\alpha = 1$ and $\hat{\mu} = 0$ mm. For that reason, the mode was eliminated from further consideration.

Table 3. The mode values $\hat{\mu}$ [mm]

μ [mm]	σ [mm]					
	0.05	0.1	0.2	0.3	0.4	0.5
0.25	0.24	0.21	0.09			
0.35	0.338	0.321	0.236	0.093		
0.5	0.495	0.48	0.42	0.32	0.18	0
1	0.998	0.99	0.96	0.91	0.84	0.75

As the samples of the ND were formed from the theoretical distributions, the method of the chi-square goodness-of-fit test [30] was used to find the difference between the empirical distributions, formed by the inversion method, and theoretical distributions. The chi-square value, χ^2, were given with number of degrees of freedom n in tab. 4, for some distribution parameters. The differences between empirical and theoretical distributions were considered acceptable because χ^2 values were smaller than the critical value $\chi^2_{n,0.05}$, where 0.05 designates the level of significance. The critical values $\chi^2_{n,0.05}$ can be found in [30].

Table 4. The χ^2 values with the number of degrees of freedom n

μ [mm]	σ [mm]					
	0.05	0.1	0.2	0.3	0.4	0.5
0.25	2602;3	3787;3	1014;3			
0.35	1959;2	4664;3	281;3	2497;3		
0.5	3840;2	5078;3	1734;3	5329;3	4592;3	
1	0107;2	2727;3	1868;3	809;3	4633;3	2171;3

Results and discussion

Radiative heat exchange was solved on a coarse numerical grid composed of the cubical volume zones of the edge dimension of 1 m. The furnace volume was divided into 7956 volume zones and furnace walls were divided into 2712 surface zones. Flow field was solved on the fine numerical grid obtained by dividing every volume zone into 64 control volumes. The agreement with the experimental data and the grid independence study were already shown [21]. The direct exchange areas of the close zones were determined using correlations given in [31]. The total exchange areas were calculated by the method of original emitters of radi-

Crnomarković, N. Dj., *et al.*: Determination of the Sootblower Activation ...
THERMAL SCIENCE: Year 2023, Vol. 27, No. 1B, pp. 755-766

761

ation [23], with the improvement of the total exchange areas using the generalized Lawson's smoothing method [32]. The total extinction coefficient and scattering albedo of the flame were 0.3 m^{-1} and 0.5, respectively. The initial wall emissivity was 0.70. For every theoretical distribution determined by the mean and standard deviation, three samples of the ND were formed. As the maximal temperatures of the outer deposit surface were about 1200 K, the ash deposits were in the condition of the loose and fused deposits.

The selected numerical results were the mean wall flux $\bar{q}_w$, as the deposits directly affect the radiative heat transfer, and flame temperature T_f, as it influences the convective heat exchange, boiler heat losses with flue gases, and NO emission.

Figure 1 shows the decrease of the mean wall flux, while figs. 2(a)-2(c) show the increase of the flame temperatures with increasing deposit thickness, in accordance with the previous investigations [16-18]. The flame gains energy from the fuel combustion, and loses energy by emission of radiation. The radiative heat exchange between the flame and furnace walls is reduced with an increase in deposit thickness, consequently as more of the internal energy remains in the flame, the flame temperature increases. The differences of the flame temperature are also caused by changes in the wall emissivity and temperature, which compose the boundary conditions for the calculation of the radiative energy transfer through the flame. Figures 1 and 2 confirm how the ash deposits affect the operation of the furnace and boiler. It reduces the radiative heat exchange in the furnace and increases the flame temperature, which increases the temperature of the superheated steam, the temperature of the waste gas at the boiler exit, and the NO concentration in the flame.
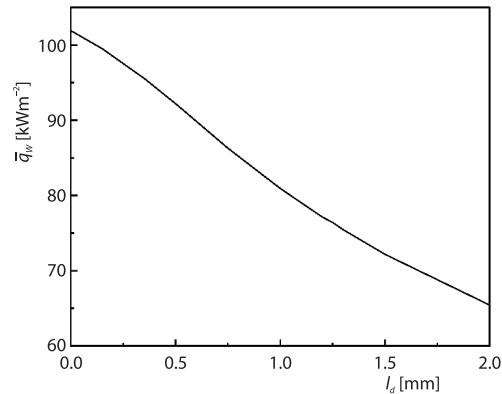

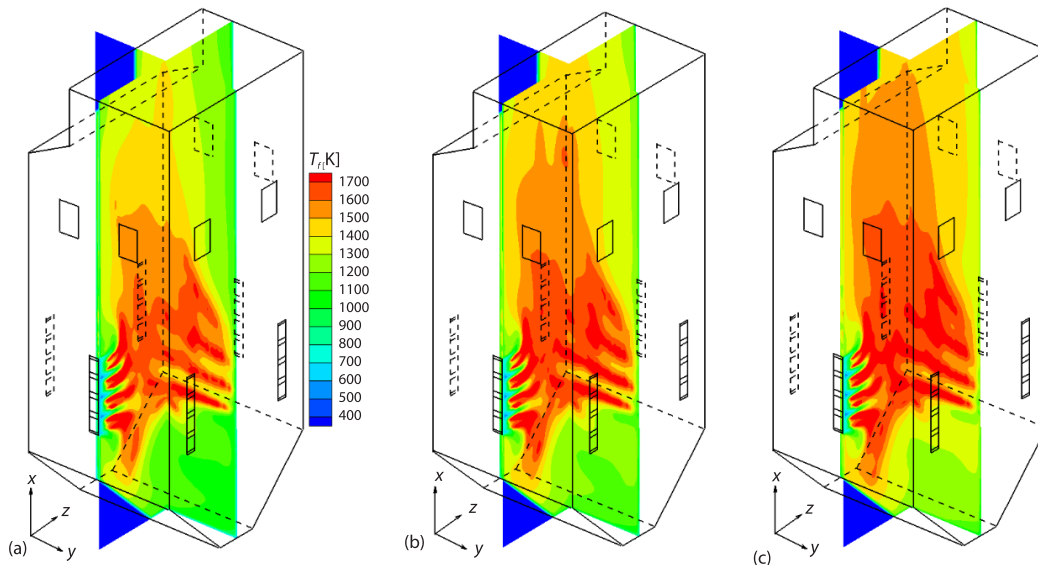**Figure 1. The mean wall flux for the UD**

Figure 2. Flame temperature for the UD; (a) $l_d = 0.15$ mm, (b) $l_d = 1$ mm, and (c) $l_d = 2$ mm

The RD of the mean wall flux for each sample were determined:

$$\overline{r} = \frac{\left| \overline{q}_{w,UD} - \overline{q}_{w,ND} \right|}{\overline{q}_{w,ND}} \qquad (5)$$

where $\overline{q}_{w,UD}$ is the mean wall flux for the UD and $\overline{q}_{w,ND}$ – the mean wall flux for the ND.

The RD of the flame temperatures for each sample were determined:

$$\overline{r} = \frac{\sum\limits_{k=1}^{ns} \dfrac{\left| T_{f,UD,k} - T_{f,ND,k} \right|}{T_{f,ND,k}}}{ns} \qquad (6)$$
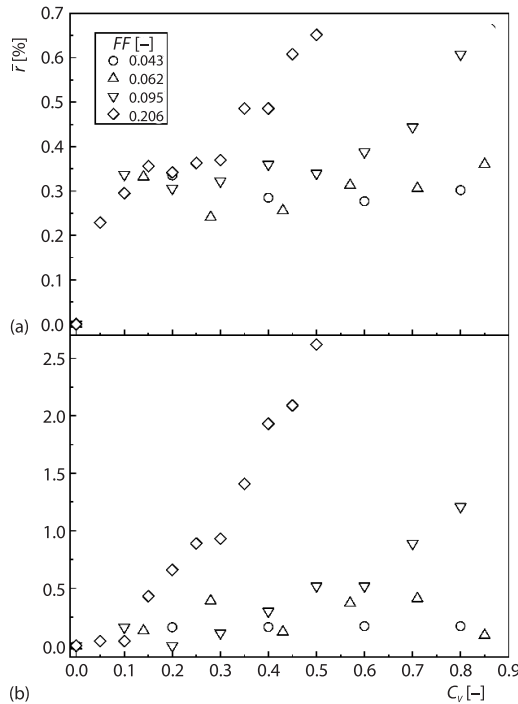
where $T_{f,UD}$ is the flame temperature determined for the UD, $T_{f,ND}$ – the flame temperature determined for the ND, and ns – the sample size, *i.e.*, the total number of the control volumes for which the flame temperatures are calculated. The RD were the averages of all three samples made for one pair of distribution parameters: $\sum \overline{r}/3$.

Whenever the effects of the ash deposits are included in numerical simulations, the results are influenced by its effective thermal conductivity. Various values of the effective thermal conductivity of the ash deposits can be found in [17, 24, 33, 34]. Higher values enable the calculation of bigger deposit thicknesses. To avoid the influence of the effective thermal conductivity on the deposit thickness, the non-dimensional fouling factor was used [35]: $FF = 1 - \overline{q}_{w,l}/\overline{q}_{w,0}$, where $\overline{q}_{w,0}$ is the mean wall flux for the clean walls and $\overline{q}_{w,l}$ is the mean wall flux for the walls covered by the UD of thickness l_d. The values of FF are the following: 0.043, for $l_{d,UD} = 0.25$ mm; 0.062, for $l_{d,UD} = 0.35$ mm; 0.095, for $l_{d,UD} = 0.5$ mm; and 0.206, for $l_{d,UD} = 1$ mm. The fouling factor FF designates UD based on the reduction of the radiative heat exchange. It was used instead of mean, as a distribution parameter. The standard deviation was presented by the non-dimensional coefficient of variation: $C_v = \sigma/\mu$. The RD of the selected variables are shown in figs. 3 and 4. When the mean of the ND is used as the UD thickness, they clearly increase with an increase in both FF and C_v. When the median is used, they depend almost only on C_v. For FF less than 0.095, *i.e.*, the thin deposits, the RD are smaller if the mean of the ND is used as the UD thickness, whereas, for FF greater than 0.095 (the thick deposits), the RD are smaller if the median is used. The median of the ND is a better choice than mean for the UD thickness, as it is more accurate for the thick deposits for which the sootblowers are activated.

It was expected that the mean of the ND would be the best selection for the UD thickness. The reason for the smaller values of the RD in the thick deposits, when the median of the ND is used as the UD thickness, can be found in the values of the local thicknesses. The mode is a point of the local maximum of the probability density function and the majority of the local thickness values are about the mode. Since the median is between the mean and mode, and as the median decreases with the increase in the standard deviation while the mean value is fixed, the RD are smaller if the median is used.

The experimental research conducted by Kupka *et al*. [14] showed that the deposit formation rates for pure coal firing and co-firing with biomass (for the biomass thermal share up to 20%) were constant for the first 140 minutes. The research showed relation between the processes of the deposit formation for co-firing with biomass and for coal firing. The present investigation was used to define a method to predict the moment of the sootblower activation, in conjunction with investigation by Kupka *et al*. [14], and the result that the rate of deposition depends on the operational regime [36]. For every operational regime planned for co-firing with biomass, the development of the ND over time should be found for pure coal firing, and the curve $\hat{\mu}(t)$ should be determined. That step contains influences of the coal composition, op-

Crnomarković, N. Dj., *et al.*: Determination of the Sootblower Activation ...
THERMAL SCIENCE: Year 2023, Vol. 27, No. 1B, pp. 755-766

763

Figure 3. The RD; (a) T_f and (b) $\overline{q}_w$; the UD thickness is a mean of the ND
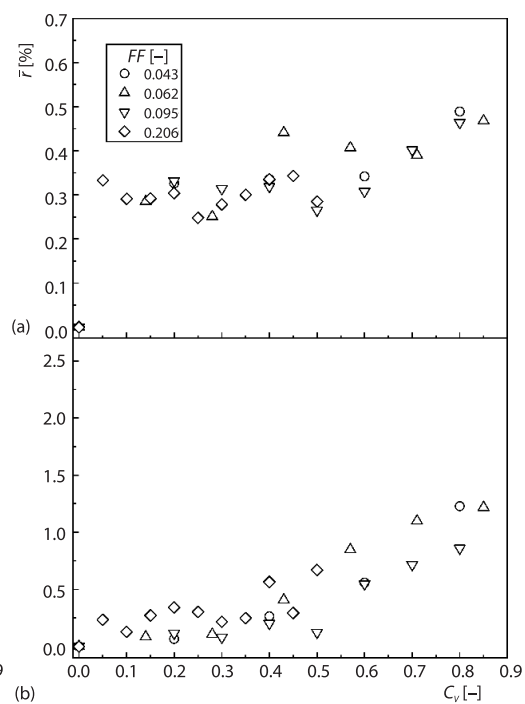
Figure 4. The RD; (a) T_f and (b) $\overline{q}_w$; the UD thickness is a median of the ND

erating conditions (number of burners in operation and their asymmetric position, boiler load, distribution of the pulverized coal along the burner, *etc.*), and furnace geometry. For co-firing, the development of the ND would need to be found for a short period of time and the median thicknesses should be found for. Then, the curve $\hat{\mu}(t)$ (for co-firing with that operational regime) can be obtained by following the shape of the curve obtained for the coal firing. The sootblowers should be activated when the maximal thickness of the UD is reached. Further research would demonstrate the entire proposed method considering particular operation regimes of the case-study utility boiler.

The whole furnace walls were considered as the sufficient number of the zones was needed for the statistical analysis. The statistical analysis can be applied to the area covered by several sootblowers or by a single sootblower, if the numerical grid must provide the sufficient number of the surface zones.

Conclusion

The relation between ND and UD, formed on the walls of the pulverized coal-fired furnace was analyzed, with the objective to apply it for determination of the sootblower activation moment for coal-biomass co-firing. The local thicknesses of the ND were determined by the gamma distribution, for several mean and standard deviations values, whereas the thicknesses of the UD were the measures of central tendency: mean, mode, and median of the ND. It was found that the median was the best choice for the thickness of the UD, as it provided the smallest values of the RDs for the thick deposits. The investigation indicated that it was possible to find the UD thickness that would provide even smaller RD. That value would be close to

Crnomarković, N. Dj., *et al.*: Determination of the Sootblower Activation ...
THERMAL SCIENCE: Year 2023, Vol. 27, No. 1B, pp. 755-766

764

the median value, and its exact value should be determined for every boiler. Based on this and previous investigations, the method to find the sootblower activation moment for coal-biomass co-firing was proposed. The idea of the method is to obtain the UD thickness development with time for the required operational regime with the co-firing, on the basis of that obtained for the same operational regime with pure coal firing. The sootblowers should be activated when the deposit reaches its maximal allowed thickness. The method could be used for the selection of the operational regimes for the coal-biomass co-firing in utility boilers which should be demonstrated in further research.

Acknowledgment

Nomenclature

A – surface area, [m^2]
C_v – coefficient of variation, [–]
F – cumulative distribution function, [–]
FF – fouling factor, [–]
f – probability density function, [mm^{-1}]
G_iS_j – volume–surface total exchange area, [m^2]
h – convection heat transfer coefficient, [Wm^{-2}K^{-1}]
K – thermal conductivity, [Wm^{-1}K^{-1}]
k – turbulent kinetic energy, [m^{2}s^{-2}]
l – thickness, [mm]
M – total number of volume zones, [–]
N – total number of surface zones, [–]
n – number of degrees of freedom, [–]
ns – sample size, [–]
Q – heat transfer rate, [W]
q – wall flux, [Wm^{-2}]
r – relative difference, [%]
S – source term
S_iS_j – surfac-surface total exchange area, [m^2]
T – temperature, [K]
t – time, [s]
$\vec{U}$ – velocity, [ms^{-1}]

Greek symbols

α – distribution coefficient, [–]
β – distribution coefficient, [mm]
Γ – transport coefficient, [kgm^{-1}s^{-1}]
$\Gamma()$ – gamma function, [–]
ϵ – emissivity, [–]

ε – turbulent energy dissipation rate, [m^{2}s^{-3}]
ζ – random number, [–]
μ – mean, [mm]
$\tilde{\mu}$ – median, [mm]
$\hat{\mu}$ – mode, [mm]
ρ – density, [kgm^{-3}]
σ – standard deviation, [mm]
σ_{SB} – Stefan-Boltzmann constant, [Wm^{-2}K^{-4}]
Φ – general gas-phase variable

Subscripts

b – boiling water
d – deposit
f – flame
fw – furnace wall
l – thickness
m – metal wall
ND – non-uniform deposit
tot – total
UD – uniform deposit
w – wall
Φ – related to general gas-phase variable

Acronyms

CCTEA – continual corrections of the total exchange areas
ND – non-uniform deposit
RD – relative difference
UD – uniform deposit

References

[1] Bhuiyan, A. A., *et al.*, A Review on Thermo-Chemical Characteristics of Coal/Biomass Co-Firing in Industrial Furnace, *Journal of the Energy Institute*, *91* (2018), 1, pp. 1-18
[2] Sahu, S. G., *et al.*, Coal-Biomass Co-Combustion: an Overview, *Renewable and Sustainable Energy Reviews*, *39* (2014), Nov., pp. 575-586
[3] Milićević, A., *et al.*, Numerical Study of Co-Firing Lignite and Agricultural Biomass in Utility Boiler under Variable Operation Conditions, *International Journal of Heat and Mass Transfer*, *181* (2021), 121728
[4] Wang, G., *et al.*, Investigation on Ash Deposit Formation during the Co-Firing of Coal with Agricultural Residues in a Large-Scale Laboratory Furnace, *Fuel*, *117* (2014), Jan., pp. 269-277

Crnomarković, N. Dj., *et al.*: Determination of the Sootblower Activation ...
THERMAL SCIENCE: Year 2023, Vol. 27, No. 1B, pp. 755-766

765

[5] Repić, B. S., *et al.*, Investigation of Ash Deposit Formation on Heat Transfer Surface of Boilers Using Coals and Biomass, *Thermal Science*, *23* (2019), Suppl. 5, pp. S1575-S1586

[6] Mladenović, M., *et al.*, Criteria Selection for the Assessment of Serbian Lignites Tendency to Form Deposits on Power Boilers Heat Transfer Surfaces, *Thermal Science*, *13* (2009), 4, pp. 61-78

[7] Mladenović, M., *et al.*, Analysis Criteria for the Assessment of Deposits Formation on Boilers Heat Transfer Surfaces during Biomass Combustion (in Serbian), *Contemporary Agricultural Engineering*, *44* (2018), 1, pp. 1-10

[8] Zhang, Y., *et a*l., *Theory and Calculation of Heat Transfer in Furnaces*, Academic Press, New York, USA, 2016

[9] Plaza, P., *et al.*, Use of a Predictive Model for the Impact of Cofiring Coal/Biomass Blends on Slagging and Fouling Propensity, *Energy and Fuels*, *23* (2009), 7, pp. 3437-3445

[10] Boardman, R., Smoot. L. D., Pollutant Formation and Control, in Fundamentals of Coal Combustion, For Clean and Efficient Use, in: *Coal Science and Technology 20*, (Ed. L. D. Smoot), Elsevier, New York, USA, 1993, pp. 433-509

[11] Kleinhans, U., *et al.*, Ash Formation and Deposition in Coal and Biomass Fired Combustion Systems: Progress and Challenges in the Field of Ash Particle Sticking and Rebound Behavior, *Progress in Energy and Combustion Science*, *68* (2018), Sept., pp. 65-168

[12] Singer, J. G., *Combustion Fossil Power*, Combustion Engineering, Monroe, Conn., USA, 1991

[13] Degereji, M. U., *et al.*, Predicting the Slagging Potential of Co-Fired Coal with Sewage Sludge and Wood Biomass, *Fuel*, *108* (2013), June, pp. 550-556

[14] Kupka, T., *et al.*, Investigation of Ash Deposit Formation during Co-Firing with Sewage Sludge, Saw-Dust and Refuse Derived Fuel, *Fuel*, *87* (2008), 12, pp. 2824-2837

[15] Frandsen, F. J., *et al.*, Deposition and Corrosion in Straw-and Coal-Straw Co-Fired Utility Boilers, Danish experiences, in: *Impact of Mineral Impurities in Solid Fuel Combustion*, (Eds. R. P. Gupta, *et al.*), Kluwer Academic/Plenum Publishers, New York, USA, 1999, pp. 271-283

[16] Ma, Z., *et al.*, A Comprehensive Slagging and Fouling Predictionol for Coal-Fired Boilers and Its Validation/Application, *Fuel Processing Technology*, *88* (2007), 11-12, pp. 1035-1043

[17] Modlinski, N. J., Computational Modelling of a Tangentially Fired Boiler with Deposit Formation Phenomena, *Chemical and Process Engineering*, *35* (2014), 3, pp. 361-368

[18] Richter, W., *et al.*, Influence of Thermal Properties of Wall Deposits on Performance of Pulverized Fuel Fired Boiler Combustion Chambers, *Proceedings*, ACS Symposium Series 301, (Ed. K. S. Vorres), American Chemical Society, Washington, USA, 1986, pp. 375-393

[19] Crnomarkovic, N. D., *et al.*, Numerical Determination of the Impact of the Ash Deposit on the Furnace Walls to the Radiative Heat Exchange inside the Pulverized Coal Fired Furnace, *Proceedings*, International Conference Power Plants 2014, Zlatibor, Serbia, 2014, pp. 1-12

[20] Crnomarkovic, N., *et al.*, Influence of Forward Scattering on Prediction of Temperature and Radiation Fields inside the Pulverized Coal Furnace, *Energy*, *45* (2012), 1, pp. 160-168

[21] Crnomarkovic, N., *et al.*, Radiative Heat Exchange inside the Pulverized Lignite Fired Furnace for the Gray Radiative Properties with Thermal Equilibrium Between Phases, *International Journal of Thermal Sciences*, *85* (2014), Nov., 2014, pp. 21-28

[22] Belosevic, S., *et al.*, Numerical Prediction of Pulverized Coal Flame in Utility Boiler Furnaces, *Energy and Fuels*, *23* (2009), 11, pp. 5401-5412

[23] Hottel, H. C., Sarofim, A. F., *Radiative Transfer*, McGraw-Hill Book, New York, USA, 1967

[24] Boow, J., Goard, P. R. C., Fireside Deposits and Their Effect on Heat Transfer in a Pulverized-Fuel-Fired Boiler – Part III: The Influence of the Physical Characteristics of the Deposit on Its Radiant Emittance and Effective Thermal Conductance, *Journal of the Institute of Fuel*, *42* (1969), 346, pp. 412-419

[25] Crnomarkovic, N., *et al.*, New Application Method of the Zonal Model for Simulations of Pulverized Coal-Fired Furnaces Based on Correction of Total Exchange Areas, *International Journal of Heat and Mass Transfer*, *149* (2020), 119192

[26] Spiegel, M. R., *et al.*, *Probability and Statistic*s, Schaum's Outline Series, McGraw-Hill, New York, USA, 2009.

[27] Larson, R. C., Odoni, A. R., *Urban Operations Research*, Prentice-Hall, New Jersey, USA, 1981

[28] ***, Keisan Online Calculator, https://keisan.casio.com

[29] Press, W. H., *et al.*, *Numerical Recipes*, Cambridge University Press, Cambridge, UK, 1986

[30] Bernstein, S., Bernstein, R., *Elements of Statistics II: Inferential Statistics*, Schaum's Outline Series, McGraw-Hill, New York, USA, 1999

[31] Tucker, R. J., Direct Exchange Areas for Calculating Radiation Transfer in Rectangular Furnaces, *Journal of Heat Transfer*, *108* (1986), 3, pp. 707-710

[32] Mechi, R., *et al.*, Extension of the Zonal Method to Inhomogeneous Non-Gray Semi-Transparent Medium, *Energy*, *35* (2010), 1, pp. 1-15

[33] Anderson, D. W., *et al.*, Effective Thermal Conductivity of Coal Ash Deposits at Moderate to High Temperatures, *Journal of Engineering for Gas Turbines and Power*, *109* (1987), 2, pp. 215-221

[34] Rezaei, H. R., *et al.*, Thermal Conductivity of Coal Ash Slags and Models Used, *Fuel*, *79* (2000), 13, pp. 1697-1710

[35] Xu, L., et al., Improvement of Slagging Monitoring and Soot-Blowing of Waterwall in a 650MWe Coal-Fired Utility Boiler, *Journal of the Energy Institute*, *96* (2021), June, pp. 106-120

[36] Tortosa-Masia, A. A., *et al.*, Slagging and Fouling in Biomass Co-Combustion, *Thermal Science*, *9* (2005), 3, pp. 85-98